

Collapse of a semiflexible polymer in poor solvent

Alberto Montesi,^{1,2} Matteo Pasquali,^{1,2,*} and F.C. MacKintosh^{2,3}

¹*Department of Chemical Engineering, Rice University, 6100 Main St., Houston, TX 77005, USA*

²*The Kavli Institute for Theoretical Physics, University of California, Santa Barbara CA 93106, USA*

³*Division of Physics and Astronomy, Vrije Universiteit, 1081 HV Amsterdam, The Netherlands*

(Dated: September 30, 2018)

We investigate the dynamics and the pathways of the collapse of a single, semiflexible polymer in a poor solvent via 3-D Brownian Dynamics simulations. Earlier work indicates that the condensation of semiflexible polymers generically proceeds via a cascade through metastable racquet-shaped, long-lived intermediates towards the stable torus state. We investigate the rate of decay of uncollapsed states, analyze the preferential pathways of condensation, and describe likelihood and lifespan of the different metastable states. The simulation are performed with a bead-stiff spring model with excluded volume interaction and exponentially decaying attractive potential. The semiflexible chain collapse is studied as functions of the three relevant length scales of the phenomenon, i.e., the total chain length L , the persistence length L_p and the condensation length $L_0 = \sqrt{k_B T L_p / u_0}$, where u_0 is a measure of the attractive potential per unit length. Two dimensionless ratios, L/L_p and L_0/L_p , suffice to describe the decay rate of uncollapsed states, which appears to scale as $(L/L_p)^{1/3} (L_0/L_p)$. The condensation sequence is described in terms of the time series of the well separated energy levels associated with each metastable collapsed state. The collapsed states are described quantitatively through the spatial correlation of tangent vectors along the chain. We also compare the results obtained with a locally inextensible bead-rod chain and with a phantom bead-spring model. Finally, we show preliminary results on the effects of steady shear flow on the kinetics of collapse.

PACS numbers: 87.15.He, 36.20.Ey, 87.15.Aa

1. INTRODUCTION AND MOTIVATION

The conformation of individual polymer chains depends on the solvent properties [1, 2, 3]. In good solvent the monomers prefer being surrounded by solvent molecules, effectively repelling each other. This effect leads to a swollen coil conformation for flexible polymers in good solvent. In poor solvent, conversely, the monomers try to exclude the solvent and effectively attract one another, and a flexible chain forms a compact globule of roughly spherical shape to minimize the contacts between monomers and solvent. The dynamics of the coil-globule transition in flexible chains are well known [4, 5, 6, 7] and involve the formation of a pearl necklace and the gradual diffusion of large pearls from the chain ends [8, 9].

Many polymers, however, exhibit substantial bending stiffness, i.e., they are semiflexible. Such polymers can be described by the worm-like chain model; examples include biopolymers (F-actin, DNA) as well as synthetic polymers (xanthan, PBO, PPTA, kevlar). Semiflexible polymers in good solvents form open, extended structures, while in poor solvent the effective self-affinity of the chain contrast this tendency and leads to chain collapse. The collapsed state configurations and the pathways to their formation are the result of the interplay between two opposing potentials: the bending potential

related to the chain stiffness and the attractive potential due to the poor solvency of the environment.

A compact globule is energetically unfavorable for semiflexible polymers because it involves highly bent states. The collapsed ground state is instead a torus, which reduces the monomer-solvent contacts without causing excessive bending penalty. Theoretical analysis [10, 11], Monte Carlo simulations [12] and experimental evidences [13, 14] have detailed the stability, the features and the packing of the collapsed tori. The dynamics of the collapse of worm-like chains in poor solvent have been investigated more recently [15, 16, 17], strongly suggesting a possible generic pathway for the collapse of semiflexible polymers, featuring a series of long-lived, partially collapsed, racquet-shaped intermediate states, before the eventual collapse to a torus. Such intermediate states form an energetically driven cascade of increasingly compact conformations with sharp transitions between their energy levels.

In the present work, we verify this hypothesis and further explore the effect of the relevant length scales on the phenomenon. The natural length scale for the polymer stiffness is its persistence length L_p , defined as the ratio of the bending stiffness κ to the thermal energy $k_B T$, which represents the length along the chain for which tangent vectors remain correlated in good solvent. The balance between attractive forces and bending forces can be considered in term of the so-called “condensation length” $L_0 = \sqrt{k_B T L_p / u_0}$, where u_0 is the value of the attractive potential per unit length. We choose as time scale for the collapse event the rotational diffusion time of a

*Electronic address: mp@rice.edu

perfectly rigid rod with $L = L_p$, $\tau_{\text{diff}, L_p} = \zeta L_p^3 / (72k_B T)$, where ζ is the transverse friction coefficient [18]. Therefore we use τ_{diff, L_p} as unit of time and $k_B T$ as unit of energy in presenting all the results of the present work. We investigate the sequences and the likelihood of different collapsed structures formed at various solvent quality (described by u_0) and chain stiffness.

2. SIMULATION DETAILS

The dynamics of the continuous wormlike chain are described by a inertialess Langevin equation:

$$\zeta \cdot \left\{ \frac{\partial \mathbf{r}}{\partial t} - \dot{\gamma} \cdot \mathbf{r} \right\} = -\frac{\delta U}{\delta \mathbf{r}} + \boldsymbol{\eta} \quad (1)$$

Equation 1 balances the hydrodynamic force exerted on the chain by the surrounding fluid with the force due to the global potential acting on the chain $U = U_{\text{bend}} + U_{\text{conn}} + U_{\text{solv}}$, and the Brownian force per unit length $\boldsymbol{\eta}$, with correlations $\langle \boldsymbol{\eta}(s, t) \boldsymbol{\eta}(s', t') \rangle = 2k_B T \zeta \delta(t - t') \delta(s - s')$. $U_{\text{bend}} = kTL_p \int_0^L ds \partial \mathbf{u}(s) / \partial s$ is the bending potential related to the chain stiffness, U_{conn} is the connector potential, U_{solv} describes the monomer-monomer interaction, and the Brownian term accounts for the rate of fluctuating momentum transfer due to the random collisions of small solvent particles with the chain.

The potential U_{solv} chosen to account for the effect of poor solvent is an exponential attractive potential with an excluded volume repulsive term:

$$U_{\text{solv}} = - \int ds \int ds' \tilde{u}_0 \exp\left(-\frac{|\mathbf{r}(s) - \mathbf{r}(s')|}{R_{\text{attr}}}\right) + \int ds \int ds' \tilde{u}_0 \left(\frac{\sigma}{|\mathbf{r}(s) - \mathbf{r}(s')|}\right)^{12}, \quad (2)$$

where \tilde{u}_0 defines the depth of the potential well, R_{attr} is the range of the attractive forces and σ is the radius of the excluded volume region. With this potential, $u_0 = R_{\text{attr}} \tilde{u}_0$. Different choices for the shape of the potential should not change the stable and metastable configurations for the wormlike chain in poor solvent, while they may modify the speed and the dynamics of the collapse. Our choice of the exponential potential is related to the physics of the condensation phenomenon. DNA and polyelectrolytes collapse because of charge inversion and counterion induced attraction [19]. The attractive forces are therefore due to highly screened electrostatic charges, which typically show an exponential decay, mimicked by the potential selected in this work.

The Brownian Dynamics code used in this work solves in dimensionless, discretized form the Langevin equation of motion of a linear wormlike chain of N beads with positions $\mathbf{R}_1, \dots, \mathbf{R}_N$, connected by $N - 1$ connectors of equilibrium length $a \equiv L / (N - 1)$ with unit tangent

vectors $\mathbf{u}_i \equiv (\mathbf{R}_{i+1} - \mathbf{R}_i) / a$. For most of the simulations reported in this work, we use quadratic springs as connectors, with a force constant equal to $100 k_B T$, which ensures a variation of the connectors' length within 30 %. This choice allows for longer time steps without interfering with the spring relaxation time. We use a midstep algorithm [20] to compute the bead trajectories generated by the equation of motion

$$\zeta_b \left\{ \frac{d\mathbf{R}_i}{dt} - \dot{\gamma} \cdot \mathbf{R}_i \right\} = \mathbf{F}_i = \mathbf{F}_i^{\text{bend}} + \mathbf{F}_i^{\text{elast}} + \mathbf{F}_i^{\text{solv}} + \mathbf{F}_i^{\text{rand}}. \quad (3)$$

Here, $\zeta_b = \zeta a$ is a bead friction coefficient, the bending force is:

$$\mathbf{F}_i^{\text{bend}} = \kappa / a \sum_{j=2}^{N-1} \partial(\mathbf{u}_j \cdot \mathbf{u}_{j-1}) / \partial \mathbf{R}_i, \quad (4)$$

the elastic force due to the spring is

$$\mathbf{F}_i^{\text{elast}} = H [(|\mathbf{u}_{i-1}| - a) \mathbf{u}_{i-1} - (|\mathbf{u}_i| - a) \mathbf{u}_i], \quad (5)$$

the potential force related to the effective interactions between the beads of the chain — repulsive within the hard core, attractive at short distance is

$$\mathbf{F}_i^{\text{solv}} = \tilde{u}_0 \sum_{j \neq i} \left[\frac{\exp(-\frac{|\Delta \mathbf{R}_{ij}|}{R_{\text{attr}}})}{R_{\text{attr}}} - \frac{12\sigma^{12}}{|\Delta \mathbf{R}_{ij}|^{13}} \right] \frac{\Delta \mathbf{R}_{ij}}{|\Delta \mathbf{R}_{ij}|} \quad (6)$$

where $\Delta \mathbf{R}_{ij} = \mathbf{R}_i - \mathbf{R}_j$, and $\mathbf{F}_i^{\text{rand}}$ is a random force.

Another relevant issue in the simulations is the accurate description of the high curvature of the collapsed states. The discretized computational model for the wormlike chain retains its validity when subsequent connectors are very nearly parallel: to satisfy this condition, a large number of connectors within the characteristic length scale of the collapsed structure is needed. The typical size of the torus and of the racquet heads are of the same order of magnitude of L_p . A good accuracy in the description of their curvature requires a large number of connectors per persistence length; for all the simulations presented here, we use 20 connectors per L_p .

We also performed simulations with a bead-rod model [21, 22], which ensures local inextensibility of the wormlike chain. The computational cost for this model is however significantly higher (~ 10 -50 times) than that for a bead-spring chain model, mainly because a smaller time step is required for convergence. While performing most of the simulations using the bead-spring model, we compared the results for a small number of conditions with the bead-rod model, as discussed in Section 3.4. In that Section we also compare some of the results with that obtained using a bead-spring phantom chain, i.e., without excluded volume interactions.

For simplicity, we use isotropic drag in the simulations, and we neglect hydrodynamic interactions between segments of the chain. Including such interactions would

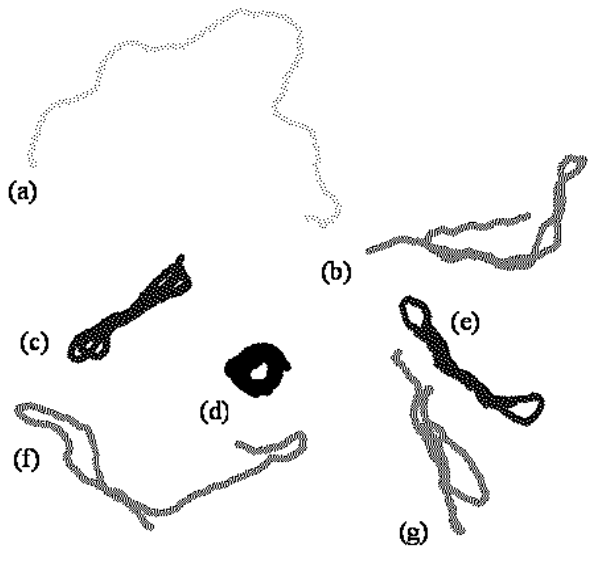


FIG. 1: Typical configurations of an ensemble of collapsing chains at an intermediate time ($L/L_p = 8$, $u_0 = 1.25kT/a$).

likely give minor corrections to the evaluation of the time scales of the phenomena, but — because at the beginning of the simulations the chains are locally straight, and because after the collapse the hydrodynamic interactions would be dominated by the attractive forces — it would not change the kinetic pathways and the relative stability of the intermediate states.

3. RESULTS

This section is organized as follows: Section 3.1 reports qualitatively the results of our simulations, describing the various possible intermediate configurations and the typical pathways. Section 3.2 presents a more quantitative description of the collapsed states in term of the correlation function between tangent vectors along the chain and of the energy levels associated with each different collapsed state, which confirm that the toroid is the stable configuration, and show how the collapse proceeds through a cascade of subsequently more energetic favorable metastable states — the various multiple headed racquets shapes, as predicted from theory [23]. The decay rate of uncollapsed states is investigated as a function of a proper combination of L , L_0 and L_p in Section 3.3, together with a statistical analysis of the preferred collapsed configurations. Section 3.4 provides a comparison between the results obtained with the different computational models (phantom chain and bead-rod chain). Some preliminary results of the effect of shear flow on the kinetics and pathways of collapse are presented in Section 3.5.

3.1. Molecule configurations and collapse pathways

Figure 1 shows a typical snapshot of an ensemble of semiflexible chains during collapse. The 3-D structures of the molecules are shown here as 2-D projections on a convenient plane. At a given time molecules coexist in different configurations, from completely uncollapsed (molecule (a)), to partially collapsed (molecules (b), (f) and (g)), to higher order racquet (molecules (c) and (e)), to toroid (molecule (d)).

The fraction of collapsed molecules increases monotonically with time, confirming that collapsed states are energetically favorable in a bad solvent. Many other ensembles with different values of L/L_p and L_0/L_p show a similar behavior. However, if the attractive forces are not strong enough or the bending stiffness is too high there is no evidence of collapse and the open conformations persist in time. As already observed in [15], a sequence of collapse can evolve following two different generic patterns. The first pattern involves the direct formation of a torus from the open conformation, when the two ends of the chain meet while the tangent vectors are locally parallel. In this instance, the chain collapses without formation of any intermediate, the end to end distance drops quickly to a value of the order of the torus dimension, and then fluctuates as the chain keeps folding into the final structure. Meanwhile the total energy of the chain keeps decreasing monotonically till reaching the equilibrium value. Conversely, the second pattern involves the formation of intermediate metastable states: initially a single racquet-headed shape which folds quickly into a short-lived, 3-heads racquet configuration, and then rearranges as a toroid via a subsequent folding. Figure 2 shows the two different pathways. We notice here that the direct formation of a torus is a more unlikely pattern in 3-D — and in fact observed with scarce frequency — than in 2-D. Whereas in 2-D the relative orientation of the two ends is described by a single angle, two angles are required in 3-D and both need to be close to 2π for the direct formation of a torus to take place. Most of the chain will therefore initially form a single headed racquet, as described below [24].

The time evolution of the total energy of an ensemble of collapsing chains is shown in Figure 3. The total energy U of the chain during collapse is defined as the sum of the bending energy U_{bend} and the interaction energy along the chain U_{solv} . In the discretized form,

$$U = kTL_p \sum_{i=1}^{N-2} \cos^2 \theta_i + \sum_{j=1}^N \sum_{k=j+1}^N u_{\text{solv},jk}, \quad (7)$$

where θ_i is the bond angle and $u_{\text{solv},jk}$ is the interaction energy evaluated between the beads j and k along the chain.

The time series in Figure 3 reports most of the possible evolutions observed in our simulations. Few molecules re-

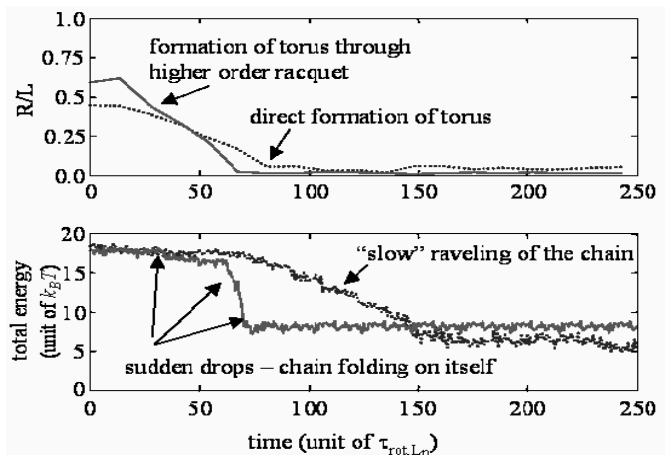


FIG. 2: Comparison between time series of end to end distance R and total energy for direct formation of toroid and formation through intermediate states.

main in the uncollapsed states for the whole duration of the run, equivalent to $250 \tau_{\text{diff}, L_p}$. For these molecules, the thermal fluctuations never lead two branches of the chain close enough together to initiate the collapse. The other molecules typically reach lower energy states by collapsing in sequentially higher order metastable conformations. The energy levels for each racquet-head shape of increasing order are well separated, and there is a rather large gap from the highest order racquet observed (6th order) and the stable tori, as expected from theory [23]. Most of the chains initially form a single head racquet: after the first monomer-monomer contact and the formation of the racquet head, the two sides of the chain tend to become parallel and form a neck region, which ensure the maximum number of monomer-monomer contacts without increasing the bending penalty. The molecules then fold again on themselves, forming higher order shapes. Depending on the way in which the molecule folds back on itself, the next configuration can be a 2-heads or a 3-heads racquet shape. Figure 3 shows examples of both pathways. Successive folding leads to higher order racquets. The transition between each single metastable conformation is very rapid and driven by the deterministic attractive and bending forces. In contrast, the initiating event for each successive collapse is related to the Brownian motion of the molecule, and therefore the time interval between folding events is extremely variable, and completely random for the simulations that we have performed. In the simulations of longer chains ($L = 10 L_p$) we observe combinations of the conformational elements described above, e.g., chains partially folded in a racquet shape at one end while still uncollapsed at the other. Those conformations have intermediate energies between the well-defined levels corresponding to racquets and tori and quickly disappear in favor of more compact and ordered structures. In contrast, the metastable high order

racquets are extremely long-lived, and the energetic barrier for reaching the equilibrium shape is of the order of several $k_B T$. While the partial unfolding of a torus in a racquet is never observed, simulations show the formation of a torus via metastable configurations, and this, together with the lower total energy shown by the torus (see Figure 3), confirms once more that the latter is the equilibrium configuration.

3.2. Quantitative description of collapsed states

The configurations and the shapes of semiflexible molecules in bad solvent can be studied through direct visualization of the collapsing chain. While this method is a valuable way to gather information on the kinetics and pathways of collapse, it is time consuming and not quantitative. We therefore define a spatial correlation matrix \mathbf{M} to analyze in a more systematic way the collapsed shapes. The elements of \mathbf{M} are defined as $M_{ij} = \mathbf{u}_i \cdot \mathbf{u}_j$. With this definition, \mathbf{M} is symmetric; a perfectly straight rod has $M_{ij} \equiv 1 \forall i, j$, as all the connecting normalized vectors have the same direction and orientation. An uncollapsed semiflexible chain with persistence length L_p will have $M_{ii} \equiv 1$, while the off-diagonal terms M_{ij} would be smaller and decaying exponentially with the distance along the chain between the connectors i and j .

When the chain collapses, the actual shape assumed by the molecule can be inferred from the spatial correlation between connectors. The spatial correlation matrix for a single head racquet, for example, will be a block matrix: one block will show values close to 1, corresponding to the almost straight filament in the neck of the racquet, followed by a region with rapidly decreasing values from 1 to -1 — the racquet head — and by another block with values close to -1 , indicating the other filament of the neck, with same direction but opposite orientation.

The spatial correlation matrix can be simplified into a spatial covariogram for the molecule. For standard statistical analysis, the covariogram is defined as

$$C(h) = 1/N(h) \sum_{j=1}^N \sum_{i=1}^N \{Z_i - \mu\} \{Z_j - \mu\} \quad (8)$$

where h is the distance (in time or in space) between the observations Z_i and Z_j , $N(h)$ is the number of observations at a distance h and μ is the expected average value of the observation. In the present analysis, for each molecule we construct the spatial covariogram C_{sp} assuming $Z_i = \mathbf{u}_i$ and $\mu = \mathbf{0}$. We therefore obtain a scalar function of the distance along the chain s , bounded between $+1$ and -1 , which contains all the relevant information about the shape of the molecule.

Figure 4 shows three relevant examples of this type of analysis: the actual shape of the semiflexible molecules

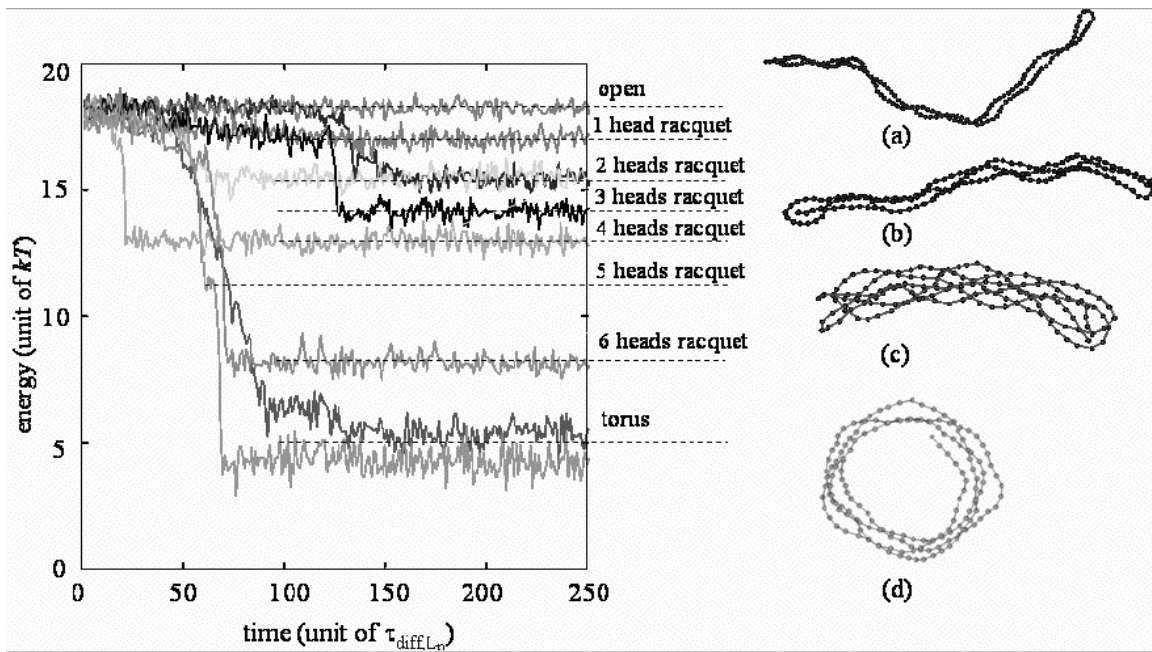


FIG. 3: Time series of total energy for an ensemble of molecules, with labels of the corresponding configurations and actual shape of (a) 1 head (b) 2 heads (c) 5 heads racquets and (d) torus.

is shown in comparison with the spatial correlation matrix and the spatial covariogram. For a uncollapsed chain (Figure 4-a), the matrix shows randomly alternating regions of positive and negative correlation along the length of the chain, corresponding to the typical open configuration of a semiflexible chain in good solvent. The corresponding covariogram shows how the connectors correlation decays from 1 to values around 0 along the length of the chain; the decay is exponential at short distances and related to the stiffness of the chain, i.e., $C_{sp} = \exp(-s/L_p)$. At longer distances, the correlation randomly oscillates between negative and positive values.

For a racquet shape with multiple heads, \mathbf{M} has a structure of alternating blocks with strong positive and strong negative correlation, as shown in Figure 4-b. The 5 straight filaments in the neck of the racquet correspond to these 5 blocks in the matrix; the size of the blocks is approximately the same and indicates the length of the racquet neck. The covariogram shows 4 zero-crossing, each corresponding to a head of the racquet, and can be fitted quite accurately with a 4th order harmonic; the parameters of this fit are related to the curvature of the racquet heads.

For a torus, the spatial correlation matrix appears completely different (Figure 4-c), showing a structure with diagonal bands. In fact, the correlation between pairs of connectors at the same distance is the same, regardless of their position along the chain; this translates into bands along the diagonals of the matrix. The distance between a diagonal with values close to 1 and one with values close to -1 corresponds to the diameter of the

collapsed torus. The same information can be extracted from the covariogram, which is a perfect sinusoid: the period of the sinusoidal function corresponds to π times the diameter of the torus, and the number of complete periods in along the chain indicates the number of loops formed by the collapsed molecule.

3.3. Kinetics of collapse

The fraction of collapsed semiflexible molecules in a bad solvent increases monotonically with time, as already stated. We have studied the effect of the relevant length scales of the phenomenon, L_p , L_0 and L , on the kinetics of this collapse. By systematically varying the total length of the chain ($L = 3L_p$, $5L_p$, $8L_p$ and $10L_p$), as well as the strength ($\tilde{u}_0 = 0.25kT/a^2$, $0.5kT/a^2$ and $1kT/a^2$) and the range ($R_{attr} = 5/40L_p$ and $1/6L_p$) of the attractive forces, we have explored the effect of these parameters on the decay rate of uncollapsed molecules. We define the time to collapse t_{coll} as the time required by the molecule to form the first metastable collapsed structure. We obtain from simulations the average value of t_{coll} in an ensemble of collapsing chain under each condition, normalized with τ_{diff, L_p} . The inverse of t_{coll} is taken as a measure of the decay rate D_{coll} of uncollapsed molecules. The distribution of the times to collapse follows the expected lognormal distribution, typical of such dynamical processes, with a peak close to the average value and a long tail.

At a given value of L/L_p , the decay rate increases,

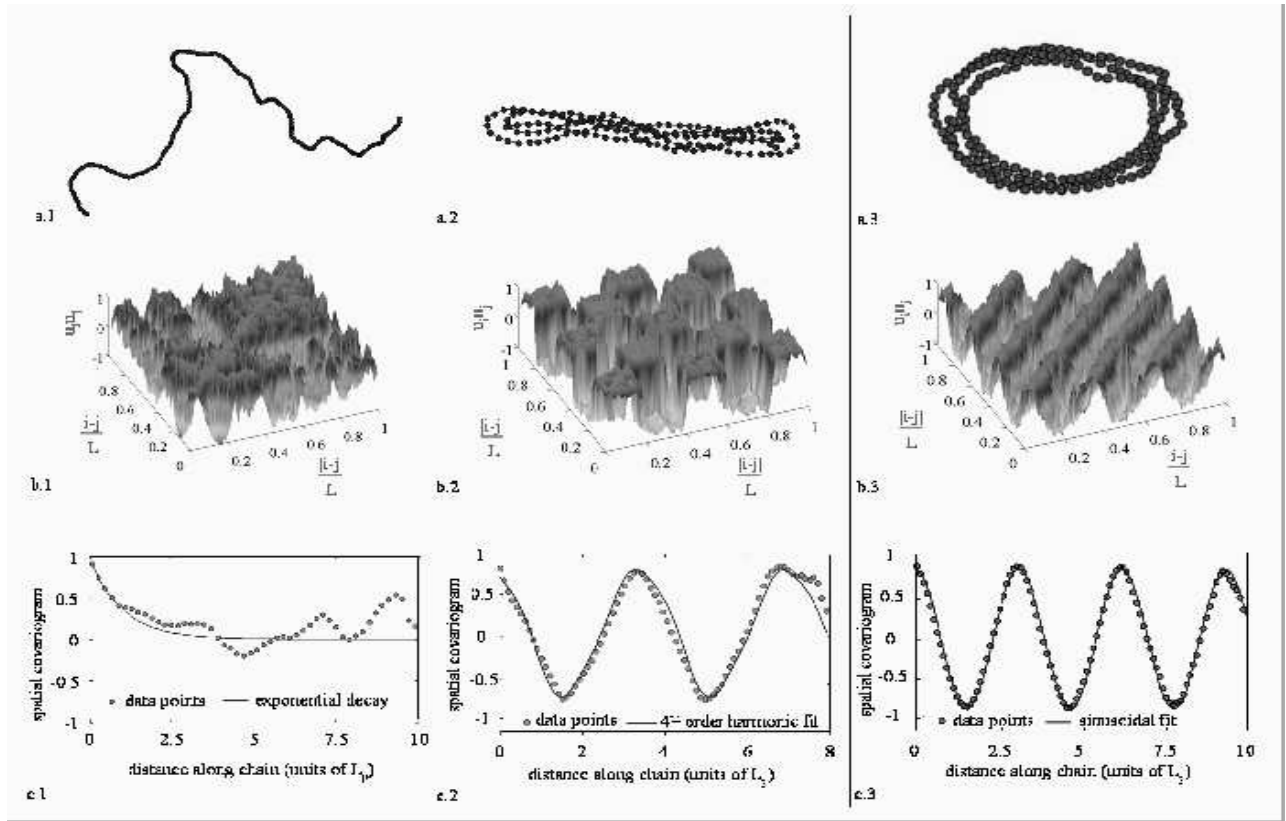


FIG. 4: (a) Actual shape, (b) correlation matrix and (c) spatial covariogram (with fitting curve) for (1) an uncollapsed molecule, (2) a metastable racquet-head shape and (3) a stable torus.

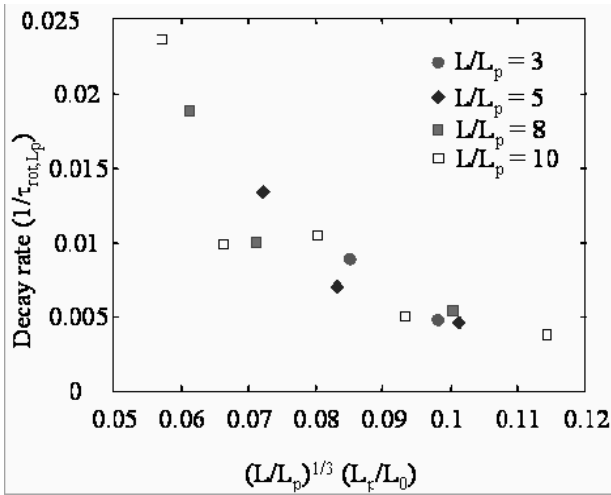


FIG. 5: Masterplot of the decay rate of uncollapsed molecules.

i.e., the molecules collapse faster, for decreasing values of L_0 , i.e., for increasing values of u_0 . Similarly, the decay rate increases for longer chains at a given value of the attractive potential and persistence length. We can collapse the values of D_{coll} on a single curve as a function of a proper combination of the two dimensionless ratios,

L/L_p and L_0/L_p , $(L/L_p)^{1/3} (L_p/L_0)$. Figure 5 shows the mastercurve for the decay rate.

Table I reports the statistics of chains conformations for different values of L/L_p at two different times, i.e., $t_1 = 100\tau_{\text{diff}, L_p}$ and $t_2 = 200\tau_{\text{diff}, L_p}$. At t_1 , the single head racquet is a conformation much more likely than the torus for all the explored values of L/L_p . This confirms that the direct formation of a torus is an unlikely event, as discussed in Section 3.1, and most of the chains collapse through a sequence of folding events. At t_2 , the percentage of molecules in the 1-head racquet configuration does not vary substantially with respect to t_1 , because — while uncollapsed molecules fold to form new 1-head racquets — some of these configurations further collapse in higher order metastable racquets and stable tori. The number of chains collapsed in tori or multiple head racquets monotonically increases within the observed span of time. For shorter chains the likelihood of tori and multiple racquets is similar, while the metastable states seem to be initially more favorable for longer chains ($L/L_p = 8$ and $L/L_p = 10$). Overall, the results show that the intermediates conformations in the collapse phenomenon are extremely long-lived: only 8.4% of the simulated chain has reached the equilibrium, torus state after $200\tau_{\text{diff}, L_p}$.

Conformation	$L/L_p = 3$		$L/L_p = 5$		$L/L_p = 8$		$L/L_p = 10$	
	t1	t2	t1	t2	t1	t2	t1	t2
open chain	62.0	43.3	48.0	30.0	43.3	36.7	49.0	36.8
single-head	31.0	43.3	36.0	42.5	33.4	30.0	24.5	23.7
multiple-heads	3.5	6.7	8.0	15.0	20.0	26.7	20.4	31.6
torus	3.5	7.9	8.0	12.5	3.4	6.7	6.1	7.9

TABLE I: Statistics of chain conformations for different L/L_p at $t1 = 100\tau_{\text{diff},L_p}$ and $t2 = 200\tau_{\text{diff},L_p}$ (% values).

3.4. Comparison of different computational models

We have performed simulation of collapsing chains with different computational models, in order to verify the results obtained and the appropriateness of the model chosen. In particular, we have performed simulations with a bead-rod model, where the chain connectors are rigid rods rather than stiff elastic spring. As noted in Section 2, the bead-rod model is a constrained model which ensures local inextensibility of the chain, but is computationally more expensive, due to more stringent time step requirements for convergence. While local inextensibility is fundamental when analyzing the polymer contribution to the stress tensor [21], its effect on the pathways and dynamics of collapse is less relevant, as confirmed by our results. In fact, we observe qualitatively similar pathways to collapse in the simulations performed with the bead-rod model. The preferred pathway includes the formation of metastable racquet shapes, similarly to what observed in the bead-spring simulations. The kinetics of the collapse are slower for the locally inextensible model; we believe that this is due to how the constraints are imposed, i.e., by projecting the random forces onto the constraints, and therefore not allowing any fluctuations along the chain. A more detailed comparison between the collapse kinetics two model is prevented by the high computational cost of simulating the constrained system.

We also perform simulations with a phantom bead-spring chain, i.e., a chain with no repulsive hard core. Once more, we find that the dynamics of collapse are qualitatively the same, although the actual shapes of the torii and of the racquets formed by the phantom chain are slightly different. The absence of hard core repulsion allows in fact for tighter structures, as shown in Figure 6. In particular, in the metastable multiple racquets the neck for phantom chains appears much narrower than for the chain where excluded volume interactions are taken into account, while it is noticeable that the shape and the curvature of the racquet head appears unchanged. The traces in time of the energy level for the phantom chain show the features already discussed in Section 3.1: well defined energy states corresponding to metastable structures, with rapid transitions between them (see Figure 6, inset). However, the average life of metastable states

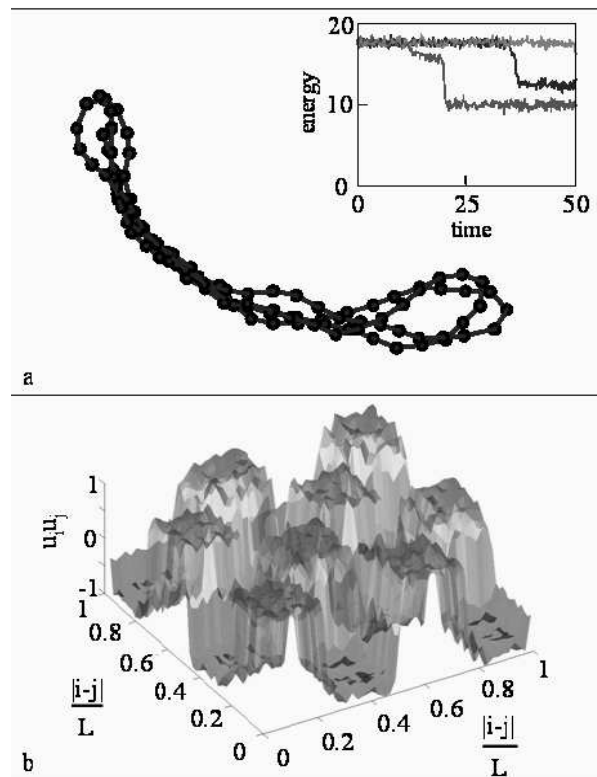


FIG. 6: (a) Metastable racquet-headed state for a phantom chain and (b) corresponding correlation matrix. Inset in (a): energy traces in time for collapsing phantom chains.

appear slightly shorter than in the complete model: intuitively, this is due to the wider range of motion of the phantom chain, which permits folding paths otherwise prevented by the excluded volume interactions.

3.5. Effect of shear flow

We discuss here the results of some preliminary work on the effects of steady shear flow on the collapse dynamics of semiflexible chains. In particular we monitor the decay rate D_{coll} at different flow strengths, and we compare the pathways of collapse with those at equilibrium. Flexible chains expand in shear flow, i.e., the average end to end distance increases while the molecules tend to orient with the flow; the effect of the flow is therefore counteracting that of the attractive forces, which tend to form compact globula. Stiff semiflexible chains, with $L_p \geq L$ shrink in shear flow, due to a buckling instability [25]; such rigid chain however would not collapse to form torii and multiple racquets in bad solvent, as the open, rod-like shape is stable at equilibrium [23]. In this work, we consider the collapse dynamics of less stiff semiflexible molecules: is not clear *a priori* what to expect for the collapse dynamics under shear flow. We show here that strong enough shear flow speeds up sen-

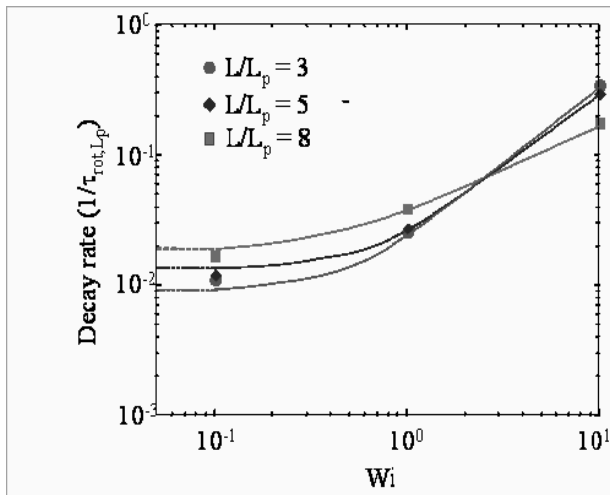


FIG. 7: Plot of the decay rate D_{coll} vs. Wi for $L/L_p = 3, 5, 8$, $\tilde{u}_0 = 1kT$ and $R_{\text{attr}} = 10/3$.

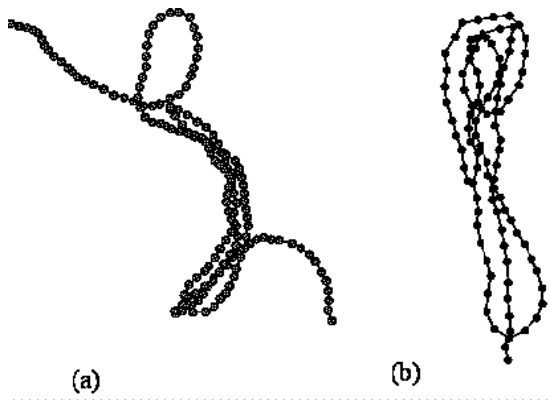


FIG. 8: Collapsed configurations of semiflexible chains in shear flow at $Wi = 10$; (a) $L/L_p = 8$, (b) $L/L_p = 5$.

sibly the collapse kinetics, increasing the likelihood for the two ends of the chain to meet. Figure 7 show the trend of the decay rate as a function of Wi , where $Wi = \dot{\gamma}\tau_{\text{diff}, L_p}$, for 3 different values of L/L_p . At $Wi = 0.1$, the decay rate does not change much with respect to the equilibrium value, and there is not a clear trend among the different L/L_p . At $Wi = 1$, the increase in decay rate becomes instead significant, as the average time to first contact halves; for $Wi = 10$, the effect of shear flow is completely dominating and the decay rate under the 3 different conditions is almost equivalent. Under shear flow, the semiflexible molecules undergo a sequence of compressions and extensions while tumbling in the plane of shear; in the compression region, the molecule tends to shrink, therefore raising the probability that two sections far apart along the chain backbone come in contact. The attractive forces then trap the molecule in the partially collapsed configuration, preventing it from straightening back in the extension region. However, this continuous

tumbling of the chain and alternation of extension and compression does not allow the formation of the higher order, compact structures observed at equilibrium. In particular, the shear flow seems to inhibit the formation of the torus, which was never observed in the high shear flow simulations. Figure 8 shows two typical configurations observed in strong shear flow; while they show the basic features of the metastable racquets, the structures are less compact and do not reach the same level of energy of the equilibrium conditions.

4. DISCUSSION

The dynamics of collapse of semiflexible molecules in bad solvent has been investigated in the literature. Direct, visual experimental evidence of the formation of torii and high order racquets has been obtained studying biopolymers with sufficiently large persistence lengths [13, 14]. Theoretical work and Monte Carlo simulations [11, 12, 23] have confirmed that the torus is the stable conformation, but intermediate, metastable racquet shaped conformations exist and are long lived. Previous Brownian Dynamics simulations in 2-D [15] have firstly suggested the possible general pathways to the dynamics of collapse.

The present work provides new insights on the collapse of semiflexible chains, confirming the suggested pathways through 3-D simulations, and showing the effect of the two relevant dimensionless ratios L/L_p and L_0/L_p on the kinetics of collapse. The time series of the total energy of each chain show clearly the fast transition between well defined energy levels, corresponding to different metastable intermediate shapes, and the final, stable torus. We also showed that two possible pathways towards the stable conformation are possible: direct formation of a torus and successive folding of the chain in progressively higher order racquets. The latter one appears to be more probable for the range of parameters investigated. The decay rate of uncollapsed states for all the different conditions of the simulation can be plotted as a function of a proper combination of L/L_p and L_0/L_p . Further work is needed to confirm the validity of this empirical scaling and verify it in a wider range of parameters.

We also performed simulations with different computational models, therefore confirming that the observed metastable conformations and pathways are general and do not depend on the choice of the model. However, the kinetics, i.e., the actual value of the decay rate can be different: in particular, for a constrained bead-rod model the kinetics of collapse appear slower, possibly due to the way the Brownian noise is projected onto the constraints.

We show preliminary results on the kinetics and pathways of collapse of semiflexible chains in shear flow. Strong enough shear flow increases the decay rate of un-

collapsed states, but prevents the formation of the compact, well defined configuration observed at rest, and seems to inhibit the formation of the torus. While these results have been obtained in unbounded shear flow, future work will consider the interaction of the collapsing molecules with a solid surface, which could be attractive or repulsive for the chain. Also, future possible direction of research include the effect of local defects along the chain, which make the molecule locally more flexible or stiffer.

The authors wish to thank Bernhard Schnurr and F. Gittes for useful discussions, and R. Adam Horch for preparing the visualizations of the collapsing DNA molecules. This work was partially supported by the National Science Foundation under grant PHY99-07949, through award CTS-CAREER-0134389 and through the Nanoscale Science and Engineering Initiative award EEC-0118007. Computational resources were provided by the Rice Parallel Computational Engineering Cluster (NSF-MRI-0116289) and by the SARA Computing and Networking Services in Amsterdam through Vrije Universiteit.

-
- [1] P. G. de Gennes, *Scaling Concepts in Polymer Physics* (Cornell University Press, Ithaca, 1979), 1st ed.
- [2] R. A. Bird, C. F. Curtiss, R. C. Armstrong, and O. Hassager, *Dynamics of Polymeric Liquids*, vol. 2 (John Wiley & Sons, New York, 1987), 2nd ed.
- [3] M. Doi and S. F. Edwards, *The Theory of Polymer Dynamics* (Oxford University Press, Oxford, 1986), 1st ed.
- [4] P. G. deGennes, *J. Phys. Lett.* **46**, 639 (1985).
- [5] B. Ostrovsky and Y. Baryam, *Europhys. Lett.* **25**, 409 (1994).
- [6] K. A. Dawson, E. G. Timoshenko, and Y. A. Kuznetsov, *Physica A* **236**, 58 (1997).
- [7] A. Halperin and P. Goldbart, *Phys. Rev. E* **61**, 565 (2000).
- [8] B. Chu, Q. C. Ying, and A. Y. Grosberg, *Macromolecules* **28**, 180 (1995).
- [9] C. F. Abrams, N. K. Lee, and S. P. Obukhov, *Europhys. Lett.* **59**, 391 (2002).
- [10] A. Y. Grosberg, *Biofizika* **24**, 32 (1979).
- [11] V. A. Bloomfield, *Biopolymers* **44**, 269 (1997).
- [12] H. Noguchi, S. Saito, S. Kidoaki, and K. Yoshikawa, *Chem. Phys. Lett.* **261**, 527 (1996).
- [13] I. Baeza, P. Gariglio, L. M. Rangel, P. Chavez, L. Cervantes, C. Arguello, C. Wong, and C. Montañez, *Biochemistry* **26**, 6387 (1987).
- [14] A. L. Martin, M. C. Davies, B. J. Rackstraw, C. J. Roberts, S. Stolnik, S. J. B. Tendler, and P. M. Williams, *FEBS Lett.* **480**, 106 (2000).
- [15] F. Schnurr, F. C. MacKintosh, and D. R. M. Williams, *Europhys. Lett.* **51**, 279 (2000).
- [16] H. Noguchi and K. Yoshikawa, *J. Chem. Phys.* **113**, 854 (2000).
- [17] T. Sakaue and K. Yoshikawa, *J. Chem. Phys.* **117**, 6323 (2002).
- [18] From slender body hydrodynamics, $\zeta = 4\pi\eta_s/\ln(L/r)$, where η_s is the solvent viscosity and L/r is the aspect ratio of the molecule.
- [19] A. Y. Grosberg, T. T. Nguyen, and B. I. Shklovskii, *Rev. Mod. Phys.* **74**, 329 (2002).
- [20] P. S. Grassia and E. J. Hinch, *J. Fluid Mech.* **308**, 255 (1996).
- [21] M. Pasquali, V. Shankar, and D. C. Morse, *Phys. Rev. E* **64**, 1 (2001), paper 020802(R).
- [22] M. Pasquali and D. C. Morse, *J. Chem. Phys.* **116**, 1834 (2002).
- [23] B. Schnurr, F. Gittes, and F. C. MacKintosh, *Phys. Rev. E* **65** (2002).
- [24] Movies showing two typical pathways, direct formation of a torus and successive folding of the chain into higher order racquets can be viewed at www.owl.net.rice.edu/~amontesi/collapsemovies.
- [25] A. Montesi, C. Wiggins, and M. Pasquali (2003), in preparation.